8740–8751 *Nucleic Acids Research, 2011, Vol. 39, No. 20* *Published online 20 July 2011*
doi:10.1093/nar/gkr578

Cytosine methylation alters DNA mechanical properties

Philip M. D. Severin[1,2], Xueqing Zou[3,4], Hermann E. Gaub[1,2,*] and Klaus Schulten[3,5,*]

[1]Lehrstuhl für Angewandte Physik and Center for Nanoscience (CeNS), Ludwig-Maximilians-Universität, Amalienstrasse 54, 80799 Munich, [2]Munich Center For Integrated Protein Science (CIPSM), Ludwig-Maximilians-Universität, Butenandtstrasse 5-13, 81377 Munich, Germany, [3]Beckman Institute, University of Illinois, Urbana, Illinois, USA, [4]School of Physics, Peking University, Beijing, China and [5]Department of Physics, University of Illinois, Urbana, Illinois, USA

Received March 27, 2011; Revised June 14, 2011; Accepted June 28, 2011

ABSTRACT

DNA methylation plays an essential role in transcriptional control of organismal development in epigenetics, from turning off a specific gene to inactivation of entire chromosomes. While the biological function of DNA methylation is becoming increasingly clear, the mechanism of methylation-induced gene regulation is still poorly understood. Through single-molecule force experiments and simulation we investigated the effects of methylation on strand separation of DNA, a crucial step in gene expression. Molecular force assay and single-molecule force spectroscopy revealed a strong methylation dependence of strand separation. Methylation is observed to either inhibit or facilitate strand separation, depending on methylation level and sequence context. Molecular dynamics simulations provided a detailed view of methylation effects on strand separation, suggesting the underlying physical mechanism. According to our study, methylation in epigenetics may regulate gene expression not only through mechanisms already known but also through changing mechanical properties of DNA.

INTRODUCTION

DNA methylation is a fundamental epigenetic mechanism of the gene-regulatory machinery in vertebrates (1–3). It occurs at the 5 position of cytosine in CpG dinucleotides, replacing a hydrogen atom by a methyl group without interfering with CG base pairing. Although methylation does not change the DNA sequence itself, strong evidence exists for a correlation between DNA methylation and alteration of gene expression (4–6). For example, in healthy cells, CG-rich regions, so-called CpG islands, of DNA are usually not methylated, but hypermethylation of CpG islands in the promoter regions of genes is often observed in cancer cells (7–9). DNA methylation also underlies genomic imprinting, where the expression of a gene depends on whether it was inherited from mother or father (10). Moreover, the pattern of DNA methylation can be stably inherited during DNA replication via maintenance DNA methyltransferases (11).

DNA methylation usually conducts transcriptional control in two ways. First, methylation prevents the binding of transcription factors to promoters, which is a simple and direct mechanism. Second, effects of DNA methylation are mediated by so-called methyl-CpG-binding domain (MBD) proteins, which recognize methylation sites on DNA (12,13). Such proteins bind to methylated DNA (mDNA) and regulate genes by further blocking the binding of RNA polymerase to the promoter (7). Although several DNA binding proteins were identified to be sensitive to methylation (14–18), the mechanism of methylation recognition is still poorly understood. Furthermore, DNA methylation can alter the structure and stability of chromatin relevant for transcriptional control of genes (19–21). For instance, nucleosomes assembled with non-methylated DNA (nDNA) appear less stable than those assembled with mDNA (22,23).

Melting curve measurements showed a minor change to higher or lower values of the melting temperature depending on the adjacent bases (24,25). In NMR experiments methylation of the CpG step was observed to reduce the dynamics of the DNA phosphate-sugar backbone (26). Molecular dynamics (MD) simulations suggest that steric hindrance and hydrophobicity of the methyl groups are causing reduced flexibility of DNA (27,28).

*To whom correspondence should be addressed. Tel: 217-244-1604; Fax: 217-244-6078; Email: kschulte@ks.uiuc.edu
Correspondence may also be addressed to Hermann E. Gaub. Tel: +49 89 2180 3172; Fax: +49 89 2180 2050; Email: gaub@physik.uni-muenchen.de

The authors wish it to be known that, in their opinion, the first two authors should be regarded as joint First Authors.

Apparently, the dynamics of DNA has an influence on protein-DNA binding specificities (29) and it is possible that methylation-induced alteration of local DNA dynamics contributes to the methylation recognition. Furthermore, prior studies suggest that methylation has an effect on the bending flexibility of DNA (30,31). Because formation of chromatin involves wrapping of DNA around the histone octamer, which requires DNA flexibility, the structure of chromatin could also be influenced by DNA methylation.

All experiments mentioned assessed thermodynamic equilibrium properties of DNA. However, the biological function of DNA involves non-equilibrium mechanical processes, such as DNA replication and transcription (32). For example, T7 DNA polymerase functions as a molecular motor and can work against a maximum DNA template tension of ~34 pN (33). DNA and RNA helicases, another type of motor protein, are involved in nearly all aspects of DNA and RNA metabolism to separate two hybridized nucleic acid strands. As recently shown, the helicases' processivity is strongly affected by forces of only a few pN (34,35). The question arises if DNA methylation has an influence on the mechanical stability of double-stranded DNA (dsDNA) under load, in particularly, on the forces needed for strand separation, which would affect translocation of helicases on DNA. In an earlier study it was shown through electromechanical experiments and simulation that cytosine methylation renders dsDNA, stretched in the electric field of a synthetic nanopore, more ordered than native dsDNA does (36).

In the present study, we conducted complementary types of force measurements using a molecular force assay (MFA) (37) and single-molecule force spectroscopy (38,39) to characterize the mechanical properties of DNA, and how they change upon methylation. Steered MD simulations (40) were carried out to characterize the influence of methylation on force-driven strand separation at atomic resolution. A strong influence of methylation on the mechanical stability of strand separation of dsDNA as well as a significant change in mechanical properties of DNA due to methylation was found in experiments. In MD simulations both mDNA and nDNA were observed to undergo a B-DNA→zipper-like DNA transition during force-induced strand separation, zipper-like mDNA containing less faults, called bubbles (41), than zipper-like nDNA does; the concentration of faults was seen to control the propensity for strand separation such that methylation influences strongly the rupture force of DNA duplexes pulled at their two 5′-ends.

METHODS

MFA DNA-chip

The DNA-chip for the MFA measurements, shown in Figure 1, has been assembled as described by Severin *et al*. (37) except for some modifications. DNA oligomers labeled **1** and **2** form the bottom duplex, oligomers **2** and **3** the top duplex.

At the bottom surface, DNA oligomer **1** is amine-modified for covalent linkage to aldehyde-functionalized glass slides. In the experiments with three methylation levels the bottom duplex **1 • 2** contained zero, one or three 5-methylcytosine (**mC**) per strand. In order to avoid artifacts in the force measurements, which could be caused by structural changes of the DNA duplex or unwanted hybridizations of the strands, we chose a well-characterized DNA sequence with minimal self-complementarity and, hence, minimal hairpin-formation (42). The top surface of the chip was a polydimethylsiloxane (PDMS) stamp, fabricated and functionalized as described previously (43,44). DNA oligomer **3** was biotinylated and linked to the stamp. The sequences of the DNA oligomers and details of the preparation of the MFA DNA-chip are provided in Supplementary Data.

MFA contact process, readout and analysis

A complete description of the overall MFA measurement can be found in a previous paper (37). A custom-built contact device is mounted on a fluorescence microscope to control contact and separation between PDMS stamp and DNA-chip via a closed-loop piezoelectric actuator. All experiments are carried out in 1× PBS (phosphate buffered saline) at room temperature. Initially, the DNA-chip and the soft PDMS stamp are separated. Cy5 is excited and the fluorescence signal (F_A^A) of the DNA-chip is measured. Subsequently Cy3 is excited and the fluorescence signal (F_D^A) of Cy5 is measured. Both surfaces are brought into contact, allowing to connect strand **3** of the MFPs to the streptavidin on the PDMS surface via biotin • streptavidin complexation (Figure 1a). After 10 min the surfaces are separated with a retract velocity of 5 μm/s and F_A^A and F_D^A read out a second time. Typically around 10^4 duplicates of molecular force probes (MFPs) are probed in parallel per μm^2.

For each pad of a stamp the four fluorescence images (F_A^A and F_D^A before contact and after separation) are analyzed to determine the normalized fluorescence intensity (NF) following (37). The NF is defined as the ratio between broken reference bonds and total amount of MFPs that have been under load and reflects the relative mechanical stability between the target duplex **1 • 2** and the reference duplex **2 • 3** of a MFP. Higher values for the NF denote an increased mechanical stability of the target duplex over the reference duplex.

Atomic force microscopy measurement and analysis

All atomic force microscopy (AFM) experiments were performed at room temperature in PBS buffer. Sample preparation is described in Supplementary Data. Spring constants k of the cantilever were determined in solution employing the expression (45,46) $k = k_B T/\langle d_C^2 \rangle$ where k_B is the Boltzmann constant, T the absolute temperature and $\langle d_C^2 \rangle$ the mean square displacement of the free cantilever end in solution. In this way typical values for spring constants of 10 to 15 pN/nm for the MLCT-C and around 70 pN/nm for the BL-AC40 were determined. The experiments were carried out with constant retract velocity and the contact time on the surface was adjusted to obtain single DNA binding events. In order to achieve satisfactory statistics, several hundred force-curves were recorded

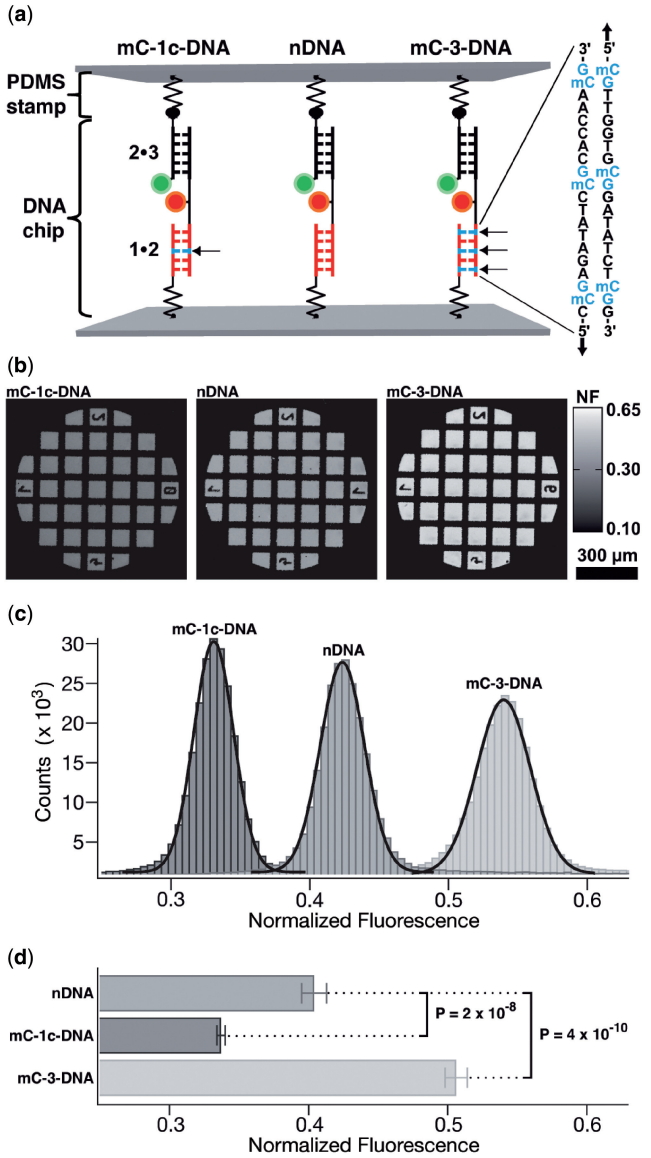

Figure 1. (**a**) Schematic representation of MFA. The MFPs are anchored via DNA strand **1** to the lower surface. Each MFP is comprised of DNA strands **1**, **2** and **3**. These three DNA strands from two DNA duplexes are coupled in series, the target duplex **1**•**2** involving nDNA, DNA with one center-methylated CpG step (mC-1c-DNA) and DNA with three methylated CpG steps (mC-3-DNA) per strand as well as a reference duplex **2**•**3**. DNA strand **2** carries a Cy5 as fluorescent marker and strand **3** a Cy3 fluorescence marker at the one end and a biotin at the other end for coupling to streptavidin on the upper surface. (**b**) NF images of one representative MFA experiment. The NF images constitute a quantitative result of the comparison of the unbinding forces between reference and target duplex. In the NF image the contacted and probed area of the PDMS stamp is clearly visible. Each pad of the PDMS stamp has a diameter of 1 mm and a microstructure of 100 µm × 100 µm. Due to the highly parallel measurement format around 10^4 MFPs are probed per µm^2. (**c**) Histograms of the three NF images in (b). The Gaussian fit of the histograms results in the following mean values and standard deviations: NF(nDNA) = (0.424 ± 0.016), NF(mC-1c-DNA) = (0.331 ± 0.014) and NF(mC-3-DNA) = (0.539 ± 0.019). (**d**) Analysis of six individual experiments. Each experiment consists on average of 4×13 analyzed pads. mC-1c-DNA shows a lower and mC-3-DNA a higher mean rupture force compared to nDNA.

for every distinct retract velocity. To obtain information about the potential width Δx and the natural dissociation rate k_{off} of the DNA duplexes, several experiments were carried out, each at a different retract velocity ranging from 150 nm/s to 20 µm/s.

The analysis of the force–extension curves was performed as described previously (47), based on the Bell-Evans-model (48,49) and using custom-made analysis software (Igor Pro 5.03, Wave Metrics). The rupture forces and corresponding loading rates of one experiment at one distinct retract velocity were plotted in two histograms, force histogram (Figure 2c) and loading rate (plotted logarithmically) histogram (Figure 2d), both fitted to a Gaussian distribution to determine the maxima of the particular histograms. These maxima were determined for each retract velocity experiment and then plotted (see Figure 2f) in a force versus loading rate (plotted logarithmically) graph; through a linear fit of the graph the natural dissociation rate at zero force and the potential width Δx of the DNA duplex were determined.

MD simulations

Non-methylated DNA (nDNA), center-methylated DNA (cDNA) and fully-methylated DNA (fDNA), as employed in the experiments, were studied in steered molecular dynamics (SMD) simulations. In each simulation, a DNA was placed in a water box of size 300 Å×60 Å×60 Å and neutralized with 100 mM KCl, amounting to 87 K^+ and 47 Cl^- ions. The resulting system is shown in Figure 3a. Each simulated system contained about 110 000 atoms. Simulations were performed using NAMD 2.6 (50). The DNA models employed and simulation details are provided in Supplementary Data.

SMD simulations, in which external forces are applied to a group of atoms, enable researchers to conduct single-molecule experiments *in silico* and see biomolecular mechanics in action. For a review of SMD simulations see (40,51,52). In our SMD simulations, one 5′-end of DNA was fixed, and the other 5′-end was pulled, as shown in Figure 3b. Three pulling conditions were applied: (i) constant velocity pulling at 10 Å/ns; (ii) constant velocity pulling at 1 Å/ns; and (iii) constant force pulling at 200 pN. In constant velocity SMD simulations, the 5′-end of DNA is attached to one end of a virtual spring; the other end of the spring is moved at a constant velocity v along the stretching x-direction and the force f applied on the 5′-end of DNA is determined through the extension of the virtual spring: $f = -k[x(t)-x(t_0)-v(t-t_0)]$. In constant force SMD simulations, a force along the stretching direction is continuously applied on the 5′-end of DNA. Five independent SMD simulations with 10 Å/ns-pulling velocity were conducted for nDNA, cDNA and fDNA; one SMD simulation with 1 Å/ns-pulling velocity covered 118 ns for each DNA; the constant force simulation covered 90 ns for nDNA and fDNA.

Due to limited computational resources, we could not employ slower pulling velocities. Because of the high pulling velocity in our SMD simulations, the rupture force of DNA seen (~1000 pN) is much higher than the

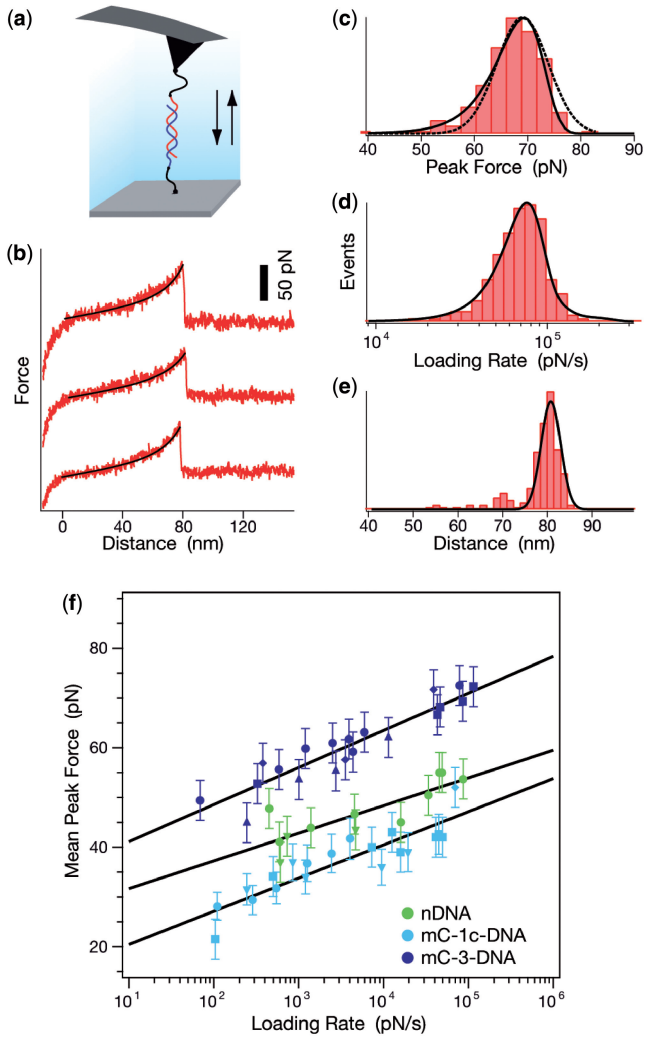

Figure 2. (**a**) Single-molecule-force-spectroscopy setup. Complementary single strands of methylated and non-methylated 20 bp DNA duplexes possessing a thiol-group at their 5′-ends were covalently immobilized on amino-functionalized glass slides and cantilevers using hetero-bifunctional PEG spacers. (**b**) Typical force–extension curves of the mC-3-DNA duplex. The force–extension curves show three sequential rupture events of a hybridized 20 bp DNA duplex, recorded at a pulling velocity of 15 µm/s. The force–extension curves of the PEG–DNA complex follow the two-state freely jointed chain-fit (black). (**c**) Typical histogram of the unbinding force of the mC-3-DNA duplex, i.e. the peak force in (b), at a pulling velocity of 15 µm/s. The histogram contains approximately 300 rupture events and the mC-3-DNA duplex dissociates at a mean force of 68 pN. The histogram is fitted with the probability density function $p(F)$ (solid curve) and a Gaussian (dotted curve). (**d**) Histogram of loadings-rates corresponding to (c); the loading rate is the slope of the curves in (b) just before the peak (rupture) force, multiplied by the pulling velocity. The histogram is fitted with the probability density function $p(F)$ (black). (**e**) Histogram of the rupture distance distribution corresponding to (c) and (d); the distance is the value corresponding to the peak force in (b). (**f**) Graph showing the most probable rupture force plotted against the corresponding most probable loading rate for nDNA, mC-1c-DNA and mC-3-DNA. The data points were gained from Gaussian fits of the rupture force histogram [see (c)] and of the histogram of the loading rates [see (d)]. Experimental results conducted with the same cantilever for nDNA, mC-1c-DNA or mC-3-DNA are depicted with one type of marker. The data points are fitted to a straight line according to the loading-rate-based analysis method yielding the values of Δx and k_{off} as given in the text.

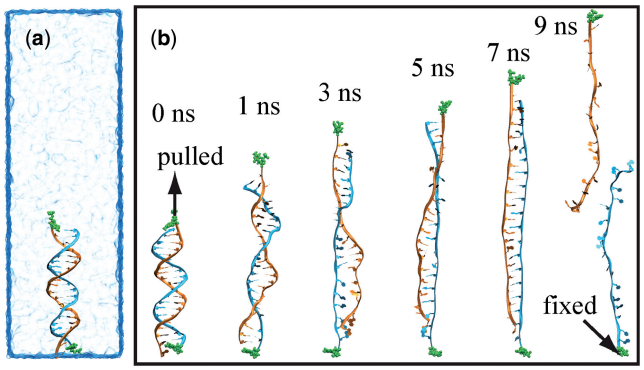

Figure 3. Strand separation of DNA under tension from simulation. (**a**) Simulated system of dsDNA in a bath of solvent and ions, as described in 'Methods' section. (**b**) Snapshots of DNA during a steered molecular dynamics simulation (simulation F1, see Supplementary Table S1). The atoms, at the 5′-end of the DNA strands, subject to constraint force (at bottom) and stretching force (at top), are highlighted in green. A movie (Supplementary Movie S1) showing the strand separation of DNA is provided in Supplementary Data.

experimental value (~100 pN). Hence, we conducted the constant force pulling SMD simulation with a force value of 200 pN for nDNA and fDNA. Supplementary Table S1 lists all the simulations carried out. The relationship of simulated and measured rupture forces has been discussed extensively by Sotomayor and Schulten (40).

The interaction free energy of DNA, e.g. base pairing and base stacking interaction, stabilizes double stranded DNA against spontaneous dissociation of two strands. Subjected to external pulling force, B-form DNA undergoes a series of conformational changes, as shown in Figure 3b. Monitoring the applied force and the length of stretched DNA in the simulations, we obtained the force–extension curve of DNA. The length of DNA is defined as the distance between the C_α atoms of the fixed 5′-end cytosine and the pulled 5′-end cytosine. To further characterize the thermodynamics of the force-induced dsDNA dissociation process, we monitored the time evolution of the number of base pairs and the stacking energy of DNA. A base pair is considered broken when the distance between hydrogen bond acceptor atom and donor atom exceeds 3 Å. Since the electrostatic contribution to DNA base stacking interaction is small (53), the stacking energy of each nucleotide was obtained by just calculating the van der Waals energy between its neighbors and itself. Most of the analysis of MD results and respective figures were prepared using the software VMD (54).

RESULTS

We first show that 5-cytosine methylation of dsDNA has a significant effect on strand separation as observed in MFA and AFM stretching experiments. To explain these findings, we examine the methylation-dependent stress-strain behavior of DNA in SMD simulations that provide a detailed view of the role of methylation on strand separation.

Determination of the mechanical stability of mDNA by MFA measurements

The MFA introduced in Figure 1 is a sensitive method to experimentally characterize DNA strand separation (37). The sensitivity of single molecule force spectroscopy by AFM, optical tweezers or magnetic tweezers is typically limited by thermal fluctuations of the force sensor. Shrinking of the sensor results in an elevated sensitivity (55) and in the MFA experiments we utilize a molecular bond as an extremely small force sensor, in our case the bonding between the strands of a DNA duplex. In fact, our MFA measurement directly compares the stability of a DNA strand duplex against the stability of a reference duplex under the same experimental (solvent, force actuator, etc.) conditions. The MFA functions here like a scale that balances a target weight against a reference weight. In comparison to common single molecule force spectroscopy, the strand separation of DNA duplexes is examined in MFA for different sequences within a single experiment due to the highly parallel format of the assay.

The experimental setup of the MFA at a molecular level consists of molecular force probes (MFPs). The MFPs are composed of two DNA duplexes, a target duplex **1 • 2** and a reference duplex **2 • 3**, which are coupled in series and connected between two surfaces (see Figure 1a and 'Methods' section). Here, the target DNA duplex is 20 bp long and contains zero (nDNA), one (mC-1c-DNA) or three (mC-3-DNA) 5-methylcytosines (mC) per strand, while the reference duplex is the same for all three different MFPs. About 10^4 MFPs per μm^2 are anchored in parallel between a glass slide (lower surface) and a PDMS stamp (upper surface). The different MFPs are immobilized as well separated spots on the glass substrate.

During separation of the two surfaces, a force builds up gradually in the MFPs until one of their two DNA duplexes ruptures, either the target duplex or the reference duplex. After separation, the ratio of ruptured target to reference duplexes is read out via the fluorescence signal of the MFPs on the lower surface and analyzed to obtain the normalized fluorescence (NF). The NF is defined as the ratio of broken reference bonds to the total amount of MFPs that have been under load. Thus, the NF is a measure for the relative mechanical stability between target and reference DNA duplexes of a MFP: a higher NF denotes a mechanical stability of the target duplex elevated over that of the reference duplex.

A representative result of a typical experiment is shown in Figure 1b, c. The Gaussian fits of the histograms of three NF-images result in the following means and standard deviations: NF(nDNA) = (0.424 ± 0.016), NF(mC-1c-DNA) = (0.331 ± 0.014) and NF(mC-3-DNA) = (0.539 ± 0.019). The difference in NF reflects a significant difference in mean rupture force between nDNA, mC-1c-DNA and mC-3-DNA.

We attribute the deviation of NF for nDNA from the expected value of 0.5 to two possible effects. First, Cy3 directly attached to the end of a DNA duplex predominantly stacks on it like an additional base pair (56) and has a stabilizing effect on the DNA duplex (57). This might lead to a more stabilized reference duplex and, thus, to a lower NF. Since all measured MFPs comprise the same reference duplex, the relative difference between the three MFPs is not influenced. Second, the MFPs are attached to different surfaces; DNA duplexes are sensitive to solution conditions such as pH value and ionic strength (58), which may differ depending on the proximity of the DNA duplex to the PDMS (top) or the glass surface (bottom). To minimize surface effects, the DNA duplexes are separated by spacers from the substrates.

After collecting results from all pads of all experiments, we determined the following NF mean values and standard errors: NF(nDNA) = (0.399 ± 0.009), NF(mC-1c-DNA) = (0.336 ± 0.003) and NF(mC-3-DNA) = (0.503 ± 0.008). The *P*-value between nDNA and mC-1c-DNA is 2×10^{-8} and for nDNA and mC-3-DNA is 4×10^{-10}. Hence, in the MFA experiments mC-1c-DNA exhibits a lower mechanical stability than nDNA, and mC-3-DNA a higher stability. Our results indicate that 5-cytosine methylation of DNA can both enhance and decrease the propensity for strand separation, the change being significant in either case.

In order to investigate how each mC-pair itself affects the mechanical stability of the DNA duplex, two more DNA constructs, mC-1u-DNA and mC-1d-DNA, were examined, each with one methylation close to one of the ends of the DNA duplex (see Supplementary Data). mC-1u-DNA and mC-1d-DNA revealed a stabilizing effect in comparison to nDNA.

Determination of potential width and dissociation constant

To further investigate the differences in strand separation of methylated and non-methylated DNA, single molecule force spectroscopy rupturing the DNA double-strand was performed by AFM, as described in 'Methods' section.

In all experiments one single-stranded DNA (ssDNA) was bound with a poly-ethyleneglycol (PEG) spacer to the cantilever tip of the AFM and a second ssDNA was immobilized with a PEG spacer on a glass substrate (see Supplementary Data). While the tip of the AFM approached the surface, the ssDNA on the tip and the ssDNA on the glass substrate could form a 20 bp duplex. The tip was then retracted from the surface and the DNA duplex was loaded with an increasing force until it finally ruptured (Figure 2a). The same sequence of the DNA duplex was used as in the MFA experiments with zero (nDNA), one (mC-1c-DNA) or three (mC-3-DNA) 5-methylcytosines (mC) per strand.

The force applied to the DNA duplex was recorded as a function of the distance between cantilever tip and surface. The elastic properties of PEG lead to a characteristic force extension curve, which can be fitted with a two-state freely jointed chain (FJC) model (Figure 2b) (59). As the complementary oligonucleotides were coupled via a PEG spacer, specific interactions can be selected based on the characteristic shape of the force–extension curve resulting from the expected length of the PEG spacer. No difference between the force–extension curve profile of nDNA, mC-1c-DNA and mC-3-DNA can be discerned.

Figure 2c and d show typical histograms of the unbinding forces and corresponding loading rates of mC-3-DNA

at a pulling velocity of 15 μm/s. The histograms contain around 300 single molecule rupture events, like those shown in Figure 2b, and are fitted to the probability density function $p(F)$ (solid curve, see 'Methods' section) and a Gaussian (dotted curve, see 'Methods' section). The most probable rupture force in Figure 2c is 68 pN. As shown in Figure 2e, the rupture events are centered in a sharp peak at a distance of around 80 nm, which matches the length of the DNA–PEG complex and is a further proof of specificity.

In Figure 2f the most probable rupture force is plotted as a function of the corresponding most probable loading rate for nDNA, mC-1c-DNA and mC-3-DNA. Measurements at faster loading rates result in higher rupture forces as described by the Bell-Evans model (48,49). By varying the pulling velocity of the cantilever from 150 nm/s to 20 μm/s, loading rates in the range of 10^2 pN/s to around 10^5 pN/s could be achieved. Each data point was obtained from the Gaussian fit of the force histogram such as the one in Figure 2c and the histogram of loading rates in Figure 2d. Due to the loading-rate-based analysis method, one can extract the potential width, Δx, and the natural dissociation rate at zero force, k_{off}, from the measurements at different pulling velocities. The following values were obtained: Δx(nDNA) = (1.66 ± 0.35) nm, k_{off}(nDNA) = (8.4×10^{-6} ± 3.52×10^{-5}) s^{-1}, Δx(mC-1c-DNA) = (1.44 ± 0.18) nm, k_{off}(mC-1c-DNA) = (1.7×10^{-4} ± 2.6×10^{-4}) s^{-1}, Δx(mC-3-DNA) = (1.24 ± 0.12) nm and k_{off}(mC-3-DNA) = (9.4×10^{-6} ± 1.72×10^{-5}) s^{-1}.

Complementing the MFA experiments, the AFM experiments reveal an elevated mechanical stability for mC-3-DNA and a decreased stability for mC-1c-DNA in comparison to nDNA. Furthermore, compared to nDNA, Δx is significantly narrower for mC-3-DNA and mC-1c-DNA. There is a slight difference in k_{off} between the three duplexes, but the error of measurement does not permit the conclusion of a significant difference.

We employed the Bell-Evans model to explain our single molecule force measurements. The Bell-Evans model assumes a single transition barrier between B-DNA and ssDNA, namely at Δx, which according to the model is force-independent. The suitability of the model has been demonstrated in several experimental studies involving force-driven strand separation of short nucleic acids (48,49,60). mC-3-DNA and mC-1c-DNA exhibit a narrower Δx in comparison to nDNA, which can be interpreted as the mDNA duplex under load to remain more compact before rupture as compared to nDNA. The narrower Δx reflects also fewer fluctuations in the mDNA corresponding to a stiffer complex.

MD simulations of DNA strand separation

When DNA is stretched in simulation, it untwists and elongates as shown in Figure 3. The dependence of the deformation on the stretching force reflects the mechanical properties of DNA. In our simulations, nDNA, cDNA and fDNA were subjected to a stretching force directed along the helical axis. Sequences of nDNA, cDNA and fDNA are provided in Supplementary Data. The trajectories of simulations carried out are available as Supplementary Movies S1–S4. Extension–force curves were monitored in slow-pulling (1 Å/ns) and fast-pulling (10 Å/ns) SMD simulations.

Figure 4 shows force–extension curves for nDNA, cDNA and fDNA stretched with a pulling velocity of 1 Å/ns. The force–extension profile exhibits in each case a clear peak followed by a rapid force decrease. The peak force arises for the extension at which the strands of the respective DNA duplex just begin to separate; the force decrease reflects the completion of strand separation. fDNA is seen to require a stronger force for strand separation than nDNA does. The force–extension curve of cDNA exhibits a minor and a major force peak. Examination of the respective simulation trajectory revealed that some flipped-out bases of the two already separated strands of cDNA stacked on each other after initial, partial separation (minor peak), as shown in critical DNA snapshots in Supplementary Figure S5. As a result, a stronger force (major peak) was needed to completely separate the DNA strands. Before DNA reaches an extension of 13.8 nm, the force–extension curves of fDNA, cDNA and nDNA are indistinguishable. However, upon further extension the force needed to extend mDNA is larger than the force needed to extend nDNA, indicating that methylation affects the late-stage of force-induced DNA strand separation.

To gain better sampling of force-induced DNA strand separation, we carried out five independent SMD simulations for nDNA, cDNA and fDNA at a pulling velocity of 10 Å/ns. Force–extension curves of the 15 simulations are shown in Figure 5. The results reveal again that the mechanical response of DNA is methylation-dependent, e.g.

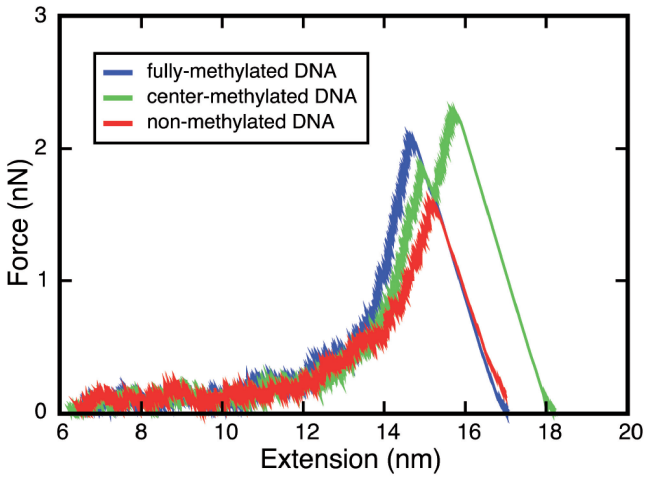

Figure 4. Force–extension curves for nDNA (red, simulation A1), cDNA (green, simulation B1) and fDNA (blue, simulation C1) when stretched by SMD with a pulling velocity of 1 Å/ns. Supplementary Figure S4 shows corresponding snapshots of nDNA, cDNA and fDNA; Supplementary Movies S2–S4 of the MD trajectories showing strand separation of nDNA (Supplementary Movie S2), cDNA (Supplementary Movie S3) and fDNA (Supplementary Movie S4) are also provided.

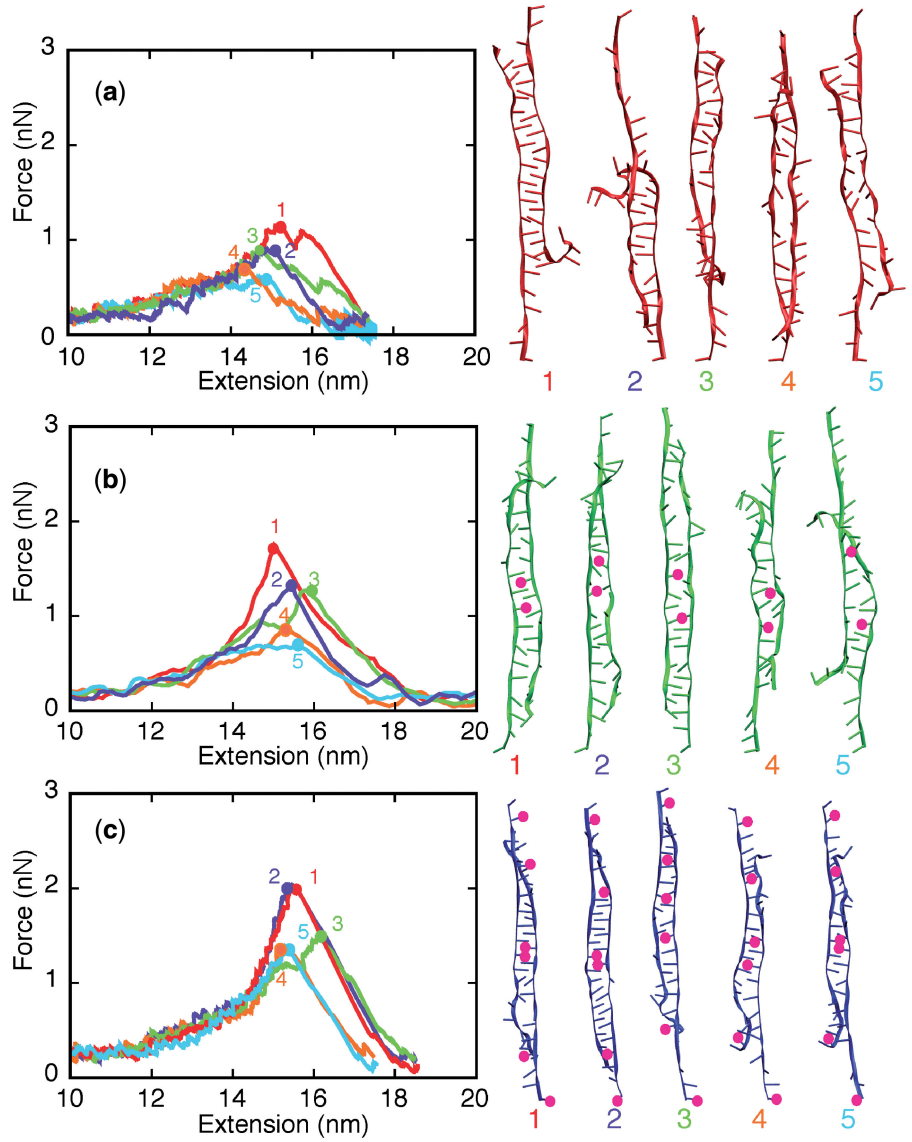

Figure 5. Force–extension curves for three different DNAs when stretched at a pulling velocity of 10 Å/ns (left) and snapshots of DNA taken at the moment of maximum stretching force (right). (**a**) nDNA with snapshots shown in red (simulations D1–D5). (**b**) cDNA with snapshots shown in green (simulations E1–E5). (**c**) fDNA with snapshots shown in blue (simulations F1–F5). In (**b**) and (**c**), magenta circles indicate the positions of methylated cytosines. For each DNA, color circles 1–5 in the force–extension curves correspond to the snapshots labeled in the same color.

DNA with more methylation sites requires a stronger force for strand separation.

During stretching, DNA undergoes a series of conformational transitions before its two strands become separated; an example is shown in Figure 3b and Supplementary Movie S1. Figure 6a shows four typical conformations of DNA that arise during force-induced strand separation in 10 Å/ns pulling simulations. The frequency of observing values of DNA length and stacking energy during 15-10 Å/ns SMD simulations are also shown in Figure 6a. Qualitatively different transition pathways between duplex state and strand separated state are observed for fDNA, cDNA and nDNA.

During the early-stage, the pathways are very similar: stretching B-form DNA induces an unwinding of the DNA helix; with the helically twisted strands straightening out into a rather planar, i.e. ladder, form, the Watson–Crick base pairing begins to break and bases of the two separate strands start to stack on top of each other, assuming the so-called zipper-like DNA form. The zipper-like DNA is demonstrated clearly in the 7 ns snapshot in Figure 3b. While the B-DNA → zipper-like DNA transition is common to fDNA, cDNA and nDNA, one can also discern differences.

First, the higher the level of DNA methylation, the less bubbles DNA develops during the B-form DNA → zipper-like DNA transition, as indicated in Figure 6a. Because of thermal fluctuation, some bases keep floating out of the zipper-like packing, and leave holes in the zipper, referred to here as 'bubbles'. The amount of

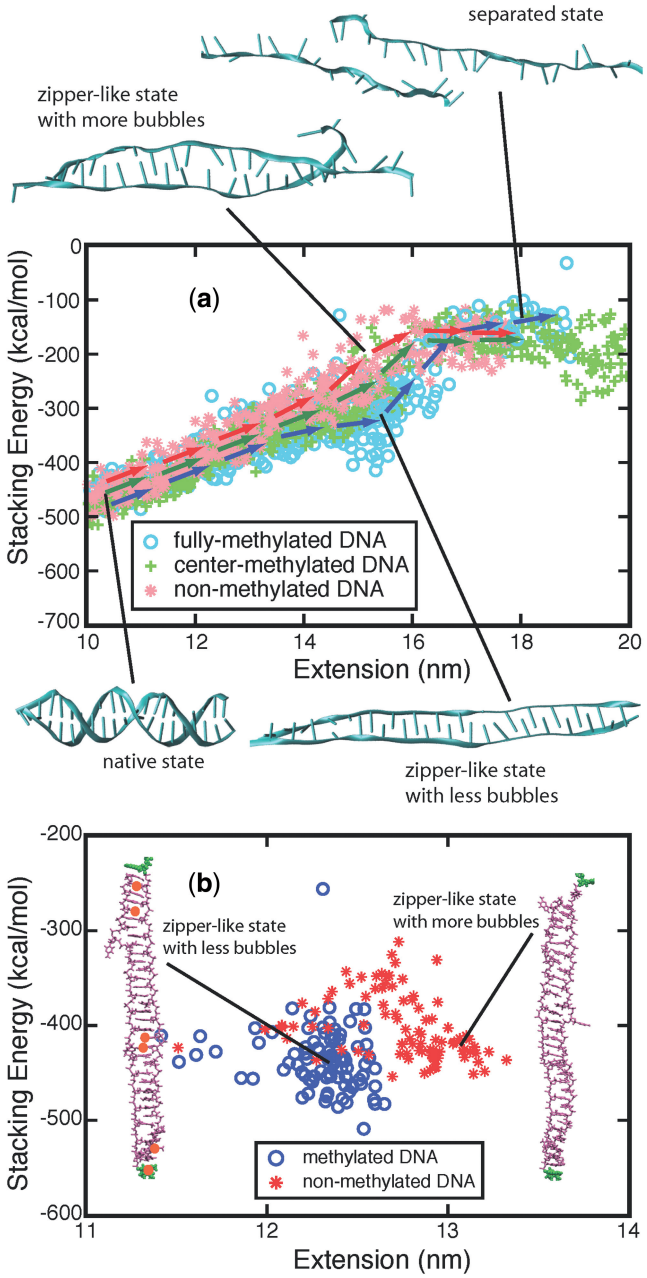

Figure 6. Strand separation pathway of stretched DNA. Here the pathway is characterized through 5′-end to 5′-end distance (extension), stacking energy of DNA bases, and intermediate DNA geometries. (**a**) Stacking energy versus extension curves of 15 trajectories of DNA pulled at 10 Å/ns velocity. Structures shown are representative snapshots taken from the simulations. Pink star: simulations D1–D5; green plus: simulations E1–E5; blue circle: simulations F1–F5. The arrows indicate three different pathways for nDNA (red arrows), cDNA (green arrows) and fDNA (blue arrows). (**b**) Stacking energy versus extension data from two 90-ns-long constant force ($F = 200$ pN) simulations pulling DNA (red, simulation G1; blue, simulation H1). mDNA adopts a shorter, ordered zipper-like conformation with fewer bubbles (left), while nDNA adopts a longer, zipper-like conformation with more bubbles (right). Orange circles indicate the positions of methylated cytosines.

developed bubbles influences the stability of DNA against strand separation. As can be seen in Figure 5, the density of bubbles, on average, is lower for DNA with more methylation sites, which is consistent with the result that fDNA requires a stronger rupture force than nDNA in our simulations.

Second, methylated ends of DNA are tighter than nonmethylated ends of DNA during stretching. The ends of most nDNAs and cDNAs are clearly separated when DNA is extended to around 15 nm, as shown in the snapshots in Figure 5. Since strand separation starts from the DNA ends under stretching, a firm end delays the separation process. As a result, rupturing DNA with methylated ends requires a stronger force than rupturing DNA without methylated ends. Supplementary Figures S6 and S7 show that the base pairing at the ends of DNA breaks more readily than that at the middle part. Methylated cytosines located at the DNA ends enable mDNA to sustain stronger force than nDNA before strands separate.

In simulations, we stretched DNA at much higher loading rates than we did in our experiments. Hence, the simulated DNA experienced a stronger pulling force and more bonds were broken in the same period of time as compared to observed DNA. To investigate the strand separation of nDNA and fDNA under conditions closer to the experimental loading force, we carried out SMD simulations at 200 pN constant force on two DNAs for 90 ns. Figure 6b shows that under 200 pN stretching, nDNA and fDNA extend along the backbone axis as the DNA increases over 90 ns its extension values. Monitoring stacking energy and length of DNA, one can distinguish two different conformational spaces occupied by nDNA and fDNA. Consistent with the strand separation pathways obtained from fast-pulling (10 Å/ns) SMD simulations, fDNA remains more compact than nDNA does. From the conformations shown in the inset of Figure 6b, one can see that zipper-like fDNA develops less bubbles than zipper-like nDNA does.

Even though we stretched dsDNA faster in MD simulations than in the experiments, the vast majority of dsDNA's degrees of freedom remain in quasi-equilibrium, fluctuating around their equilibrium values. The quasi-equilibrium behavior results from the fast relaxation of atomic velocities ($\tau_{relax} \approx 100$ fs) and of local conformational features, e.g. bond angles or weak and medium hydrogen bonding with $\tau_{relax} \approx 1 - 100$ ps. The relaxation times are short compared with the simulation times adopted here, of 10−100 ns and, hence, the stretched DNA remains in quasi-equilibrium during the simulations. However, there exist also relevant slow degrees of freedom in the stretched dsDNA system, namely the faults referred to above as bubbles. The faults are instrumental for strand separation and exhibit relaxation times on the order of nanoseconds as can be seen in the Supplementary Movies S1–S4. The 'slow' degrees of freedom lead to the heterogeneity of the simulation results as seen in Figure 5 and 6. The relaxation behavior of fast degrees of freedom has been discussed in (61). A key slow degree of freedom, essential for strand separation of protein β-sheets, has been reported in (62) and monitored over many orders of magnitude of stretching velocities in experiment and simulation as discussed in (63).

DISCUSSION

It has been well recognized that DNA methylation conducts its biological function either, at a local level, by affecting promoter regions to recruit repressor complexes and, thereby, to induce transcriptional silencing, or at a genome-wide level, by changing structure and stability of chromatin to influence gene activity (19,20,22,23). In the last case, although MBD proteins are always involved in formation of higher inactive chromatin structure, methylation might also exert its biological effects by itself, e.g. without interfering with transcription factor and MBD protein binding, through a mechanical influence on DNA. In a previous study, it was demonstrated that methylation affects DNA's electromechanical properties (36). In the present work, we investigated the effect of 5-cytosine methylation on mechanical properties of DNA under load through force-induced strand separation measurement and simulation. The methylation-dependent strand separation behavior has been identified in MFA and AFM experiments; the underlying physical mechanism has been investigated by MD simulation.

MFA measures the relative stability of a target DNA duplex versus a reference DNA duplex during strand separation. In comparison with nDNA, the probability of strand separation for mC-3-DNA is approximately (NF(mC-3-DNA)−NF(nDNA))/NF(nDNA) = 26% lower and for mC-1c-DNA ∼19% higher. Since mC-3-DNA, mC-1c-DNA and nDNA were measured in parallel, spatially separated in the same well, their measurement conditions were identical. Hence, the measured differences in the strand separation probability between mC-3-DNA, mC-1c-DNA and nDNA are highly reliable. Complementing the MFA experiments, single molecule force measurements reveal distributions and absolute values of rupture forces as well as the corresponding loading rates. As shown in Figure 2f, compared to nDNA, mC-3-DNA has a higher mean rupture force (31% at 3 nN/s) and mC-1-DNA a lower mean rupture force (19% at 3 nN/s), which is in agreement with a higher (lower) likelihood of DNA strand separation for mC-1c-DNA (mC-3-DNA) relative to nDNA in the MFA measurements.

SMD simulations, by examining force–extension curves, confirmed the dependence of strand separation on cytosine methylation, the method being limited, though, to small sampling. Three significantly different separation pathways were identified for nDNA, cDNA and fDNA by monitoring length and stacking energy of DNA during strand separation. The differences are attributed to the enhanced stacking interaction between methylated cytosine and its adjacent bases. Indeed, the stacking energy increases due to the additional methyl group on cytosine, reduces internal bubble formation and tightens the ends of DNA. As a result, to rupture mDNA requires stronger force than to rupture nDNA.

In all SMD simulations, we applied pulling velocities of 1 Å/ns and 10 Å/ns, which are several orders of magnitude higher than experimental pulling velocities (1.0×10^{-6} Å/ns ∼1.0×10^{-4} Å/ns). Using a higher velocity increases the speed of strand separation, allowing simulations to finish within the timescale (∼100 ns) that our computational resources permit. The pulling velocity influences the rupture force of DNA as described for three protein systems (40). The reference demonstrates along with (63) that despite differences in pulling speed SMD simulation identified the correct physical rupture mechanisms. In our MD simulations, we could observe at atomic detail how methylation affects DNA strand separation in each independent simulation. While the simulations also show a clear difference between non-methylated and mDNA rupture forces, the main value of the results derives from the detailed picture of the strand separation process provided. In this picture, DNA duplexes are stretched into a zipper-like conformation; the eventual strand separation occurs due to random faults, here called bubbles, arising in this conformation; once enough bubbles weaken strand–strand interaction, based mainly on stacking energy contributions, separation occurs. Under the slow pulling conditions of the experiments, reaching a critical concentration of bubbles is rare, i.e. happens only over a millisecond; under the fast pulling condition of the simulations, strain favors bubble formation such that the critical concentration sufficient for strand separation is reached in 100 ns. The zipper-like DNA duplex conformation had been seen in several earlier simulation studies of nDNA (64,65), and some NMR studies have observed that zipper-like DNA can exist stably (66,67); the critical role of bubbles in strand separation has been described by Rapti *et al.* (41).

Experiments and simulations demonstrated methylation-dependent behavior of DNA during stand separation. However, comparing experimental and simulation results directly, one can notice that for cDNA, experiments showed that methylation reduces the force demand for strand separation, while simulations showed the opposite. The discrepancy between experiment and simulation should be attributed to the small sampling in MD simulations. For a low methylation level, such as cDNA with only one methylcytosine per strand, the effect of methylation is minor and easily drowned in noise. For fDNA, simulations more readily catch the effect of methylation. In fact, for fDNA, MD simulation results are indeed consistent with experimental results: methylation increases the requirement on force to separate strands. Due to limited computational power, MD simulations presently cannot sample as much as experiments can; nevertheless, MD simulation can provide key mechanistic insights complementing single-molecule experiments (40).

The goal of our study was to elucidate the methylation effect on physical properties of DNA. Comparison of strand separation of DNA with different methylation patterns illustrates that the effect of cytosine methylation is not only dependent on the methylation level, e.g. fDNA requires the strongest force for strand separation, but also on the sequence context of methylated sites, e.g. despite the same number of methylated cytosine, the relationship $\text{stability}_{\text{mC-1u-DNA}} > \text{stability}_{\text{nDNA}} > \text{stability}_{\text{mC-1c-DNA}}$ holds (see Supplementary Figure S1). Previous studies had demonstrated significant sequence-dependence for biological functions of DNA, for example, one induced

through abnormal conformations as in the case of $(CA)_n$ DNA tracts (68,69).

Complementing our results on DNA mechanical stability, melting curve experiments allow the determination of thermal stability. Methylation-sensitive high-resolution melting curve experiments allow an investigation of the methylation level affecting DNA duplex thermal stability in bulk (25). Lefebvre *et al*. (24) reported that methylation increases the melting temperature (T_m) in the case of the DNA sequence ATCGAT by 3 K, while T_m decreases by 1 K for the sequence TTCGTT. This sequence-dependent effect of cytosine methylation on thermal DNA stability agrees with the sequence-dependent effect in our study of the mechanical stability. DNA methylation taking the same effect in two different transitions, namely force-induced strand separation in our study and temperature-induced melting in prior studies, suggests that methylation effects can be manipulated by the quantity and the context of methylation sites.

In contrast to the subtle changes of methylation effects as seen typically in thermal stability measurements, the differences in mechanical stability arising from methylation are pronounced, which prompts the question if this effect has a biological function. In this respect we note that the processivity of helicases is strongly affected by forces of a few picoNewton (34,35). Recently, Johnson *et al*. (70) showed in single-molecule force measurements that DNA strand separation is the major barrier in T7 helicase translocation. Moreover, the strand separation rate of helicase T7 is DNA sequence-dependent and strongly influenced by a force stretching the DNA. Here, we measured a mean rupture force increase of 14 pN (at 3 nN/s) for mC-3-DNA over nDNA.

Of course, the force applied in our experiments differs from the force arising *in vivo* in the case of helicases, as we measured strand separation in shear geometry. We note, however, that mechanical manipulation of DNA in transcription initiation occurs in the confined setting of highly structured polynucleosomes. Accordingly, the shear geometry motion, which has been experimentally probed and computationally visualized in our study and which takes place more or less within the volume of non-stretched DNA, is relevant in the rather compact, structured polynucleosome setting found in the cell nucleus.

We have explored also DNA strand separation through unzipping, applying forces which may seem more representative of the action of DNA helicases. Such separation poses more spatial requirements than does strand separation through shearing as Supplementary Movie S5 representing a simulation shows. We have carried out MFA measurements and MD simulations in unzipping geometry for the same sequences and under the same conditions as for the shear geometry. The MFA experimental setup and results are shown in Supplementary Figure S2; Supplementary Figure S3 shows results of a simulation of DNA being unzipped. As one can see from Supplementary Figure S2, NF mean values and standard errors are (0.501 ± 0.002) for nDNA, (0.511 ± 0.003) for mC-1c-DNA and (0.583 ± 0.004) for mC-3-DNA, i.e. methylation effects overall are significantly less than those arising in the case of strand separation in shear geometry. The same is true in the case of the simulation results and we conclude that DNA unzipping shows likely a weaker methylation dependence than does strand separation through shearing.

In summary, we have demonstrated that cytosine methylation has a significant effect on DNA strand separation. We also suggested a microscopic picture of how strand separation arises in our experiments and how methylation plays a role on DNA strand separation in principle. There are three main mechanisms of the transcriptional regulation of gene expression: chromatin structure controlled access to genes, transcription factor control and epigenetic influence. DNA methylation, by adding a single methyl group on cytosine, is proven to be essential in epigenetics. Our study reveals that methylation could regulate gene expression through changing DNA mechanical properties. This new finding may advance our understanding of methylation-based epigenetics.

SUPPLEMENTARY DATA

Supplementary Data are available at NAR Online.

ACKNOWLEDGEMENTS

The authors thank B. Gaub, J. Vogelsang and M. Erdmann for helpful discussions. K.S. and X.Z. are grateful to G. Timp for introducing them to epigenetics. P.S. is grateful to the Elite Network of Bavaria (IDK-NBT) for a doctoral fellowship. K.S. is grateful for a Humboldt Foundation award. The authors gladly acknowledge supercomputer time provided by the Texas Advanced Computing Center and the National Center for Supercomputing Applications via TeraGrid Resource Allocation Committee grant MCA93S028.

FUNDING

Deutsche Forschungsgemeinschaft; Nanosystems Initiative Munich; German Science Foundation (SFB 863); National Institutes of Health (P41-RR005969, R01 GM073655); National Science Foundation (PHY0822613). Funding open access charge: National Institutes of Health (P41-RR005969, R01 GM073655).

Conflict of interest statement. None declared.

REFERENCES

1. Bird,A.P. (1992) The essentials of DNA methylation. *Cell*, **70**, 5–8.
2. Jones,P.A. and Takai,D. (2001) The role of DNA methylation in mammalian epigenetics. *Science*, **293**, 1068–1070.
3. Bonasio,R., Tu,S. and Reinberg,D. (2010) Molecular signals of epigenetic states. *Science*, **330**, 612–616.
4. Razin,A. and Riggs,A.D. (1980) DNA methylation and gene function. *Science*, **210**, 604–610.
5. Rottach,A., Leonhardt,H. and Spada,F. (2009) DNA methylation-mediated epigenetic control. *J. Cell. Biochem.*, **108**, 43–51.

6. Maunakea,A.K., Nagarajan,R.P., Bilenky,M., Ballinger,T.J., D'Souza,C., Fouse,S.D., Johnson,B.E., Hong,C., Nielsen,C., Zhao,Y. *et al.* (2010) Conserved role of intragenic DNA methylation in regulating alternative promoters. *Nature*, **466**, 253–257.
7. Baylin,S.B. and Herman,J.G. (2000) DNA hypermethylation in tumorigenesis: epigenetics joins genetics. *Trends Gen.*, **16**, 168–174.
8. Tsou,J.A., Hagen,J.A., Carpenter,C.L. and Laird-Offringa,I.A. (2002) DNA methylation analysis: a powerful new tool for lung cancer diagnosis. *Nat. Oncogene*, **21**, 5450–5461.
9. Jones,P.A. (2002) DNA methylation and cancer. *Oncogene*, **21**, 5358–5360.
10. Li,E., Beard,C. and Jaenisch,R. (1993) Role for DNA methylation in genomic imprinting. *Nature*, **366**, 362–365.
11. Stein,R., Gruenbaum,Y., Pollack,Y., Razin,A. and Cedar,H. (1982) Clonal inheritance of the pattern of DNA methylation in mouse cells. *Proc. Natl Acad. Sci. USA*, **79**, 61–65.
12. Ballestar,E. and Wolffe,A.P. (2001) Methyl-CpG-binding proteins. *Eur. J. Biochem.*, **268**, 1–6.
13. Straussman,R., Nejman,D., Roberts,D., Steinfeld,I., Blum,B., Benvenisty,N., Simon,I., Yakhini,Z. and Cedar,H. (2009) Developmental programming of CpG island methylation profiles in the human genome. *Nat. Struct. Biol.*, **16**, 564–571.
14. Wakefield,R.I., Smith,B.O., Nan,X., Free,A., Soteriou,A., Uhrin,D., Bird,A.P. and Barlow,P.N. (1999) The solution structure of the domain from MeCP2 that binds to methylated DNA. *J. Mol. Biol.*, **291**, 1055–1065.
15. Ohki,I., Shimotake,N., Fujita,N., Jee,J.-G., Ikegami,T., Nakao,M. and Shirakawa,M. (2001) Solution structure of the methyl-CpG binding domain of human MBD1 in complex with methylated DNA. *Cell*, **105**, 487–497.
16. Hashimoto,H., Horton,J.R., Zhang,X., Bostick,M., Jacobsen,S.E. and Cheng,X. (2008) The SRA domain of UHRF1 flips 5-methylcytosine out of the DNA helix. *Nature*, **455**, 826–829.
17. Avvakumov,G.V., Walker,J.R., Xue,S., Li,Y., Duan,S., Bronner,C., Arrowsmith,C.H. and Dhe-Paganon,S. (2008) Structural basis for recognition of hemi-methylated DNA by the SRA domain of human UHRF1. *Nature*, **455**, 822–825.
18. Ho,K.L., McNae,L.W., Schmiedeberg,L., Klose,R.J., Bird,A.P. and Walkinshaw,M.D. (2008) MeCP2 binding to DNA depends upon hydration at methyl-CpG. *Mol. Cell*, **29**, 525–531.
19. Hashimshony,T., Zhang,J., Keshet,I., Bustin,M. and Cedar,H. (2003) The role of DNA methylation in setting up chromatin structure during development. *Nat. Genet.*, **34**, 187–192.
20. Lorincz,M.C., Dickerson,D.R., Schmitt,M. and Groudine,M. (2004) Intragenic DNA methylation alters chromatin structure and elongation efficiency in mammalian cells. *Nat. Struct. Biol.*, **11**, 1068–1075.
21. Choy,J.S., Wei,S., Lee,J.Y., Tan,S., Chu,S. and Lee,T.-H. (2010) DNA methylation increases nucleosome compaction and rigidity. *J. Am. Chem. Soc.*, **132**, 1782–1783.
22. Kass,S.U., Pruss,D. and Wolffe,A.P. (1997) How does DNA methylation repress transcription? *Trends Gen.*, **13**, 444–449.
23. Keshet,I., Lieman-Hurwitz,J. and Cedar,H. (1986) DNA methylation affects the formation of active chromatin. *Cell*, **44**, 535–543.
24. Lefebvre,A., Mauffret,O., Antri,S.E., Monnot,M., Lescot,E. and Fermandjian,S. (1995) Sequence dependent effects of CpG cytosine methylation. A joint 1H-NMR and 31P-NMR study. *Eur. J. Biochem.*, **229**, 445–454.
25. Wojdacz,T.K., Dobrovic,A. and Hansen,L.L. (2008) Methylation-sensitive high-resolution melting. *Nat. Protocol.*, **3**, 1903–1908.
26. Geahigan,K.B., Meints,G.A., Hatcher,M.E., Orban,J. and Drobny,G.P. (2000) The dynamic impact of CpG Methylation in DNA. *Biochemistry*, **39**, 4939–4946.
27. Mayer-Jung,C., Moras,D. and Timsit,Y. (1998) Hydration and recognition of methylated CpG steps in DNA. *EMBO J.*, **17**, 2709–2718.
28. Derreumaux,S., Chaoui,M., Tevanian,G. and Fermandjian,S. (2001) Impact of CpG methylation on structure, dynamics and solvation of cAMP DNA responsive element. *Nucleic Acids Res.*, **29**, 2314–2326.
29. Hogan,M.E. and Austin,R.H. (1987) Importance of DNA stiffness in protein-DNA binding specificity. *Nature*, **329**, 263–266.
30. Meints,G.A. and Drobny,G.P. (2001) Dynamic impact of methylation at the M. HhaI target site: a solid-state deuterium NMR study. *Biochemistry*, **40**, 12436–12443.
31. Nathan,D. and Crothers,D.M. (2002) Bending and flexibility of methylated and unmethylated EcoRI DNA. *J. Mol. Biol.*, **316**, 7–17.
32. Bustamante,C., Chemla,Y.R., Forde,N.R. and Izhaky,D. (2004) Mechanical processes in biochemistry. *Annu. Rev. Biochem.*, **73**, 705–748.
33. Wuite,G.J., Smith,S.B., Young,M., Keller,D. and Bustamante,C. (2000) Single-molecule studies of the effect of template tension on T7 DNA polymerase activity. *Nature*, **404**, 103–106.
34. Cheng,W., Dumont,S., Tinoco,I. and Bustamante,C. (2007) NS3 helicase actively separates RNA strands and senses sequence barriers ahead of the opening fork. *Proc. Natl Acad. Sci. USA*, **104**, 13954–13959.
35. Dumont,S., Cheng,W., Serebrov,V., Beran,R.K., Tinoco,I. Jr, Pyle,A.M. and Bustamante,C. (2006) RNA translocation and unwinding mechanism of HCV NS3 helicase and its coordination by ATP. *Nature*, **439**, 105–108.
36. Mirsaidov,U.M., Timp,W., Zou,X., Dimitrov,V., Schulten,K., Feinberg,A.P. and Timp,G. (2009) Nanoelectromechanics of methylated DNA in a synthetic nanopore. *Biophys. J.*, **96**, L32–L34.
37. Severin,P., Ho,D. and Gaub,H.E. (2011) A high-throughput molecular force assay for protein-DNA interactions. *Lab Chip*, **11**, 856–862.
38. Clausen-Schaumann,H., Seitz,M., Krautbauer,R. and Gaub,H.E. (2000) Force spectroscopy with single bio-molecules. *Curr. Opin. Cell Biol.*, **4**, 524–530.
39. King,G.M., Carter,A.R., Churnside,A.B., Eberle,L.S. and Perkins,T.T. (2009) Ultrastable atomic force microscopy: atomic-scale stability and registration in ambient conditions. *Nano Lett.*, **9**, 1451–1456.
40. Sotomayor,M. and Schulten,K. (2007) Single-molecule experiments in vitro and in silico. *Science*, **316**, 1144–1148.
41. Rapti,Z., Smerzi,A., Rasmussen,K.Ø. and Bishop,A.R. (2006) Healing length and bubble formation in DNA. *Phys. Rev. E*, **73**, 051902.
42. Strunz,T., Oroszlan,K., Schäfer,R. and Güntherodt,H.-J. (1993) Dynamic force spectroscopy of single DNA molecules. *Proc. Natl Acad. Sci. USA*, **96**, 11277–11282.
43. Albrecht,C.H., Clausen-Schaumann,H. and Gaub,H.E. (2006) Differential analysis of biomolecular rupture forces. *J. Phys.: Condens. Matter*, **18**, 81–599.
44. Ho,D., Dose,C., Albrecht,C.H., Severin,P., Falter,K., Dervan,P.B. and Gaub,H.E. (2009) Quantitative detection of small molecule/DNA complexes employing a force-based and label-free DNA-microarray. *Biophys. J.*, **96**, 4661–4671.
45. Butt,H.J. and Jaschke,M. (1995) Calculation of thermal noise in atomic-force microscopy. *Nanotechnology*, **6**, 1–7.
46. Florin,E.L., Rief,M., Lehmann,H., Ludwig,M., Dornmair,C., Moy,V.T. and Gaub,H.E. (1995) Sensing specific molecular interactions with the atomic force microscope. *Biosen. Bioelectron.*, **10**, 895–901.
47. Morfill,J., Kühner,F., Blank,K., Lugmaier,R.A., Sedlmair,J. and Gaub,H.E. (2007) B-S transition in short oligonucleotides. *Biophys. J.*, **93**, 2400–2409.
48. Bell,G. (1978) Models for the specific adhesion of cells to cells. *Science*, **200**, 618–627.
49. Evans,E. and Ritchie,K. (1999) Strength of a weak bond connecting flexible polymer chains. *Biophys. J.*, **76**, 2439–2447.
50. Phillips,J.C., Braun,R., Wang,W., Gumbart,J., Tajkhorshid,E., Christophe Chipot,E.V., Skeel,R.D., Kale,L. and Schulten,K. (2005) Scalable molecular dynamics with NAMD. *J. Comp. Chem.*, **26**, 1781–1802.
51. Gao,M., Sotomayor,M., Villa,E., Lee,E. and Schulten,K. (2006) Molecular mechanisms of cellular mechanics. *Phys. Chem. Chem. Phys.*, **8**, 3692–3706.
52. Isralewitz,B., Gao,M. and Schulten,K. (2001) Steered molecular dynamics and mechanical functions of proteins. *Curr. Opin. Struct. Biol.*, **11**, 224–230.

53. Friedman,R.A. and Honig,B. (1992) The electrostatic contribution to DNA base-stacking interactions. *Biopolymers*, **32**, 145–159.
54. Humphrey,W., Dalke,A. and Schulten,K. (1996) VMD – visual molecular dynamics. *J. Mol.Graph.*, **14**, 33–38.
55. Viani,M.B., Schäffer,T.E., Chand,A., Rief,M., Gaub,H.E. and Hansma,P.K. (1999) Small cantilevers for force spectroscopy of single molecules. *J. Appl. Physiol.*, **86**, 2258–2262.
56. Iqbal,A., Arslan,S., Okumus,B., Wilson,T.J., Giraud,G., Norman,D.G., Ha,T. and Lilley,D.M.J. (2008) Orientation dependence in fluorescent energy transfer between Cy3 and Cy5 terminally attached to double-stranded nuclelic acids. *Proc. Natl Acad. Sci. USA*, **105**, 11176–11181.
57. Harvey,B.J., Perez,C. and Levitus,M. (2009) DNA sequence-dependent enhancement of Cy3 fluorescence. *Photochem. Photobio. Sci.*, **8**, 1105–1110.
58. Rouzina,I. and Bloomfield,V.A. (2001) Force-induced melting of the DNA double helix 2. Effect of solution conditions. *Biophys. J.*, **80**, 894–900.
59. Oesterhelt,F., Rief,M. and Gaub,H.E. (1999) Single molecule force spectroscopy by AFM indicates helical structure of poly(ethylene-glycol) in water. *New J. Phys.*, **1**, 1998–1999.
60. Ho,D., Zimmermann,J.L., Dehmelt,F.A., Steinbach,U., Erdmann,M., Severin,P., Falter,K. and Gaub,H.E. (2009) Force-driven separation of short double-stranded DNA. *Biophys. J.*, **97**, 3158–3167.
61. Hsin,J. and Schulten,K. (2011) Improved resolution of tertiary structure elasticity in muscle protein. *Biophys. J.*, **100**, L22–L24.
62. Lu,H. and Schulten,K. (2000) The key event in force-induced unfolding of titin's immunoglobulin domains. *Biophys. J.*, **79**, 51–65.
63. Lee,E.H., Hsin,J., Sotomayor,M., Comellas,G. and Schulten,K. (2009) Discovery through the computational microscope. *Structure*, **17**, 1295–1306.
64. Lohikoski,R., Timonen,J. and Laaksonen,A. (2005) Molecular dynamics simulation of single DNA stretching reveals a novel structure. *Chem. Phys. Lett.*, **407**, 23–29.
65. Santosh,M. and Maiti,P.K. (2009) Force induced DNA melting. *J. Phys. Condens. Matter*, **21**, 101–139.
66. Shepard,W., Cruse,W.B., Fourme,R., de la Fortelle,E. and Prangè,T. (1998) A zipper-like duplex in DNA: the crystal structure of d(GCGAAAGCT) at 2.1 Å resolution. *Structure*, **6**, 849–861.
67. Chou,S.-H. and Chin,K.-H. (2001) Zipper-like Watson-Crick base-pairs. *J. Mol. Biol.*, **312**, 753–768.
68. Timsit,Y., Vilbois,E. and Moras,D. (1991) Base-pairing shift in the major groove of $(CA)_n$ tracts by B-DNA crystal structures. *Nature*, **354**, 167–170.
69. Timsit,Y. and Moras,D. (1995) Self-fitting and self-modifying properties of the B-DNA molecule. *J. Mol. Biol.*, **251**, 629–647.
70. Johnson,D.S., Bai,L., Smith,B.Y., Patel,S.S. and Wang,M.D. (2007) Single-molecule studies reveal dynamics of DNA unwinding by the ring-shaped T7 helicase. *Cell*, **129**, 1299–1309.